7-19-2022

The role of the parenchymal vascular system in cerebrospinal fluid tracer clearance

Jiani Hu

Yimin Shen

Lara M. Fahmy
Henry Ford Health, lfahmy1@hfhs.org

Satish Krishnamurthy

Jie Li

See next page for additional authors

Recommended Citation
Hu J, Shen Y, Fahmy LM, Krishnamurthy S, Li J, Zhang L, Chen Y, Haacke EM, and Jiang Q. The role of the parenchymal vascular system in cerebrospinal fluid tracer clearance. Eur Radiol 2022.

European Radiology
https://doi.org/10.1007/s00330-022-09022-9

MAGNETIC RESONANCE

The role of the parenchymal vascular system in cerebrospinal fluid tracer clearance

Jiani Hu[1] · Yimin Shen[1] · Lara M. Fahmy[2,3] · Satish Krishnamurthy[4] · Jie Li[4] · Li Zhang[2] · Yongsheng Chen[5] · E. Mark Haacke[1] · Quan Jiang[2,5]

Received: 26 January 2022 / Revised: 21 June 2022 / Accepted: 4 July 2022

Abstract

Objectives The current understanding of cerebral waste clearance (CWC) involves cerebrospinal fluid (CSF) participation but lacks convincing evidence for the direct participation of the parenchymal vascular system. The objective of this study was to evaluate the role of the parenchymal vascular system in CSF tracer clearance in rats.

Methods We used superparamagnetic iron oxide–enhanced susceptibility-weighted imaging (SPIO-SWI) and quantitative susceptibility mapping (QSM) methods to simultaneously study 7 T MRI signal changes in parenchymal veins, arteries, and their corresponding para-vascular spaces in 26 rats, following intra-cisterna magna (ICM) infusion of different CSF tracers (FeREX, Ferumoxytol, Fe-Dextran) to determine the amount of tracer in the artery and vein quantitatively.

Results We observed that the parenchymal venous system participated in CSF tracer clearance following ICM infusion of different MRI tracers with different concentrations of iron. Parenchymal venous participation was more obvious when 75 μg iron was injected. In the parenchymal veins, the relative mean (± SE) value of the susceptibility increased by 13.5 (± 1.0)% at 15 min post-tracer infusion ($p < 0.01$), and 33.6 (± 6.7)% at 45 min post-tracer infusion ($p = 0.01$), compared to baseline. In contrast to the parenchymal veins, a negligible amount of CSF tracer entered the parenchymal arteries: 1.3 (± 2.6)% at 15 min post-tracer infusion ($p = 0.6$), and 12 (± 19)% at 45 min post-tracer infusion ($p = 0.5$), compared to baseline.

Conclusions MRI tracers can enter the parenchymal vascular system and more MRI tracers were observed in the cerebral venous than arterial vessels, suggesting the direct participation of parenchymal vascular system in CWC.

Key points

- *MRI results revealed that the parenchymal venous system directly participates in cerebrospinal fluid tracer clearance following ICM infusion of MRI tracer.*
- *Different sizes of MRI tracers can enter the parenchymal venous system.*

Keywords Rats · Glymphatic system · Cerebral veins · Contrast media · Magnetic resonance imaging

Abbreviations

aROI	Arterial region-of-interest
azicv	Azygos internal cerebral vein
azp	Azygos pericallosal artery
BBB	Blood–brain barrier
CNS	Central nervous system
CSF	Cerebrospinal fluid
CWC	Cerebral waste clearance
ICM	Intracisternal magna
IV	Intravenous

Jiani Hu and Yimin Shen contributed equally to this work.

✉ E. Mark Haacke
nmrimaging@aol.com

✉ Quan Jiang
qjiang1@hfhs.org

[1] Department of Radiology, Wayne State University, Detroit, MI, USA

[2] Department of Neurology, Henry Ford Health System, 2799 W Grand Blvd, Detroit, MI 48202, USA

[3] Department of Psychiatry and Behavioral Neurosciences, Wayne State University, Detroit, MI, USA

[4] Department of Neurosurgery, Upstate Medical University, Syracuse, NY, USA

[5] Department of Neurology, Wayne State University, Detroit, MI, USA

Published online: 19 July 2022

MRI	Magnetic resonance imaging
PVS	Peri-venous space
QSM	Quantitative susceptibility mapping
ROI	Region-of-interest
SI	Signal intensity
SPIO	Superparamagnetic iron oxide
SPIO-SWI	Superparamagnetic iron oxide–enhanced susceptibility-weighted imaging
SWI	Susceptibility-weighted imaging
vROI	Venous region-of-interest

Introduction

Impaired cerebral waste clearance (CWC) has been associated with a broad range of both physiological and pathophysiological neurologic conditions in animal studies, making it a focus-of-interest and an important area of study [1–9]. The brain has long been considered to be devoid of a conventional lymphatic system. Studies in the last decade [1–3, 10–12] have fundamentally altered the traditional model of cerebrospinal fluid (CSF) hydrodynamics and led to the conceptualization of a system responsible for the removal of interstitial fluid (ISF) out of the brain, mostly from peri-venous pathways. This system has become known as the glymphatic system [7, 10] and provides a pathway for an organized convective fluid flow that drives clearance of interstitial solute from the brain parenchyma. A large proportion of subarachnoid CSF enters the interstitium through periarterial pathways and exchanges with ISF (CSF-ISF exchange), and both are cleared together with any associated solutes along specific peri-venous pathways [1]. Because of the unique anatomy of the brain parenchyma, biochemically inert waste such as MRI contrast agents can only be removed through two possible pathways: a cerebrospinal fluid (CSF) pathway and/or a vascular pathway. Although controversy exists in the efflux pathways [1, 8, 13, 14], there seems to be solid consensus about the participation of the CSF pathway in CWC.

In addition to the CSF pathway, the vascular system can play a role in helping with CWC. Invoking the vascular system as the major CWC pathway for non-specific substances via the arachnoid granulations was published by Weed et al over 100 years ago. Challenging this concept are novel insights utilizing molecular and cellular biology as well as neuroimaging, which indicate that a direct transfer of molecules from the CSF to the venous system via arachnoid granulations is up for debate [9, 15]. Several studies [9, 15–18] have clearly demonstrated that there is rapid transport of the macromolecules into the blood stream from the brain parenchyma other than from the arachnoid granulations. However, these studies cannot identify the contribution of the vascular system in CWC. Consequently, a key question about CWC remains controversial without solid supportive data: whether non-specific waste with different sizes can be directly removed by the brain parenchymal vascular system. There are far more studies on how substances in the vascular system enter the brain, rather than on how substances are removed from the brain via the vascular pathway [19–21].

The major challenge in answering the question lies in the need for an imaging tool that quantitatively measures tracer influx and efflux in micro-vessels and their surroundings. In order to address this critical need, we used superparamagnetic iron oxide (SPIO)–enhanced susceptibility-weighted imaging (SWI, SPIO-SWI) to study this problem [22–25]. The SPIO-SWI method capitalizes on the combination of the SWI blooming effect (local signal loss from the presence of magnetic field gradients) and the SPIO contrast agent's high susceptibility, in order to significantly increase the detection sensitivity of sub-pixel micro-vessels. This should provide the capability to distinguish between contributions from the peri-vascular versus intra-vascular spaces. The objective of this study was to determine whether MRI tracers in the brain parenchyma can directly enter the parenchymal vascular system following an intracisternal magna (ICM) infusion.

Materials and methods

All experimental procedures were conducted and performed in accordance with guidelines of the National Institute of Health (NIH) for animal research under a protocol approved by the Institutional Animal Care and Use Committees of Wayne State University, and experimental guidelines of ARRIVE (items 8, 10 to 13). All experimental procedures were approved by the Institutional Animal Care Committee of Wayne State University.

Experimental design

Figure 1a illustrates the logic behind the experimental design in a simplified format: if tracers in the parenchymal arteries and tracers in the parenchymal veins can be simultaneously measured, we can determine whether there is tracer entering the parenchymal vascular system from the parenchyma by comparing the amount of influx tracers in arteries with efflux tracers in veins, even without knowing how tracers enter or exit the parenchymal vascular system.

Animal studies

A total of 26 adult (3–4 months) male Wistar rats (350–450 g) were used for the MRI studies (Fig. 1b). Five rats were used

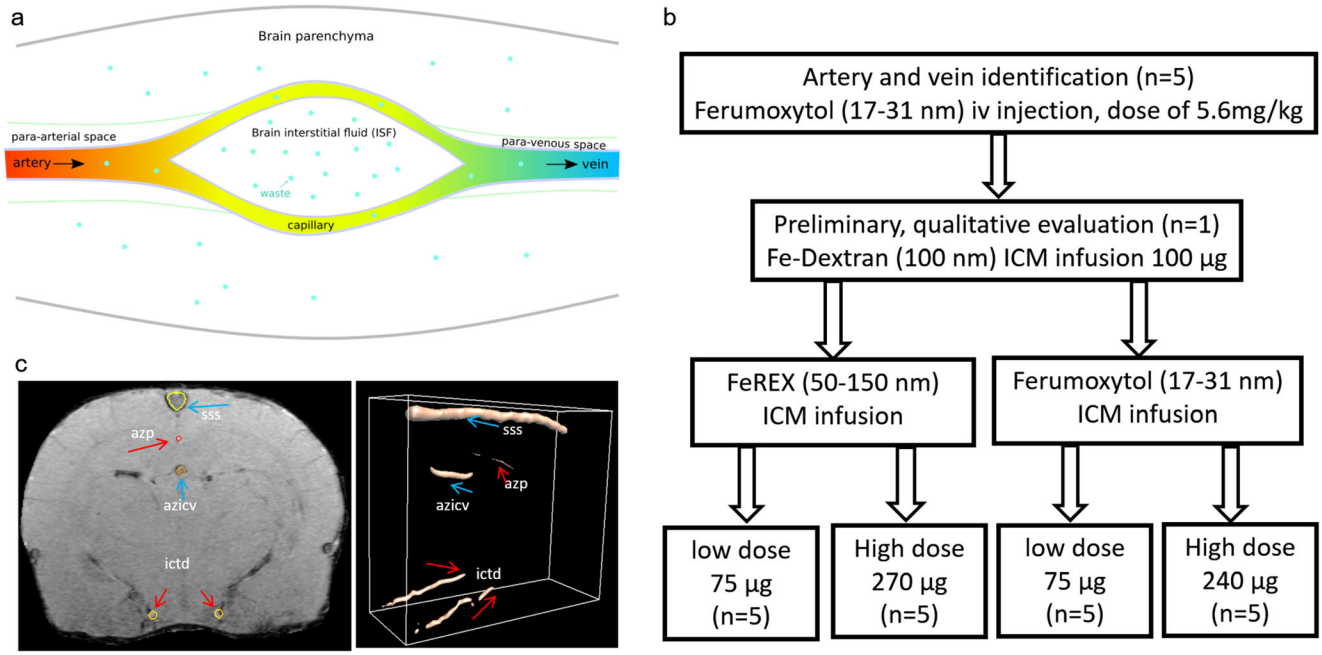

Fig. 1 **a** Illustration of the experimental design in a simplified format. Regardless of how tracers enter or exit the brain parenchyma, a net increase in the efflux tracers of the parenchymal vein compared to the influx tracers of the parenchymal artery indicates that the tracers enter the parenchymal vascular system. More specifically, there appears to be a net increase in the veins but not in the arteries. **b** Experimental flowchart. **c** Illustration of vessels of interest in 2D (left) and 3D (right)

to identify the artery and vein used in this study with IV injection of Ferumoxytol at the optimized dosage of 5.6 mg/kg and to verify the experimental protocol (Fig. 2c). One rat was used to confirm our previous optimized protocol for Fe-Dextran [9] and the capability of the SPIO-SWI method to simultaneously distinguish parenchymal arteries, veins, and corresponding para-vascular spaces (Fig. 2d–i). A total of 20 rats were used to determine whether MRI tracers in the brain parenchyma can directly enter the parenchymal vascular system with an ICM infusion of Ferumoxytol or FeREX using different concentrations of iron (Fig. 1b).

MRI experiments

Intra-cisterna magna infusion Unless intravenous administration was indicated, MRI tracers were administered via an ICM infusion based on published studies documenting the optimized MRI infusion rate and a dosage to produce reliable MRI data [26, 27]. Briefly, we had infused the CSF tracer at an optimized rate of 1.67 µL/min for 54 min using a 100-µL syringe (Hamilton Robotics), leading to a total infusion volume of about 90 µL CSF tracer.

MRI tracers All tracers were superparamagnetic iron oxide–based: Ferumoxytol (Feraheme, AMAG Pharmaceuticals Inc.), FeREX™ (BioPAL Inc.), and Fe-Dextran (nanomag®-CLD-redF, micromod-Partikeltechnologie GmbH). Ferumoxytol is an iron replacement product used clinically in the treatment of anemia; it is a non-stoichiometric magnetite (superparamagnetic iron oxide (SPIO)) coated with polyglucose sorbitol carboxymethylether. Its overall colloidal particle size is 17–31 nm in diameter. FeREX™ is an SPIO having an iron core of approximately 5 nm. The size of the resulting colloidal matrix ranges from 50 to 150 nm. Fe-Dextran consists of cross-linked dextran iron oxide composite particles with a size of 100 nm in diameter. The original iron concentrations were 30 mg/mL in Ferumoxytol, 10 mg/mL in FeREX™, and 2.4 mg/mL in Fe-Dextran. Tracers were saline-diluted to achieve appropriate dosing. Tracers were either injected intravenously or ICM.

MRI measurements MRI measurements were performed with a 7-T system (ClinScan; Bruker) on anesthetized rats laying on a warming cradle with the temperature set to 38°C. The dynamic tracer influx and clearance process was monitored using a multi-echo 3D SWI scan [28]. For Ferumoxytol and FeREX™ tracers, we used echo times of 5.22 ms, 12.97 ms, and 20.71 ms; repetition time of 60 ms; flip angle of 15°; field-of-view of 19 × 19 × 31 mm^3 (read, phase, slice) in a coronal orientation; matrix size of 384 × 192 × 192 (which yielded a resolution of 50 × 100 × 160 μm^3); and an acquisition time of 30 min. For the Fe-Dextran tracer, we used echo times of 2.69 ms and 7.71 ms; repetition time of 60 ms; flip angle of 15°; field-of-view of 16 × 16 × 28.16 mm^3 in a coronal orientation; matrix size of 384 × 192 × 176 (which yielded an

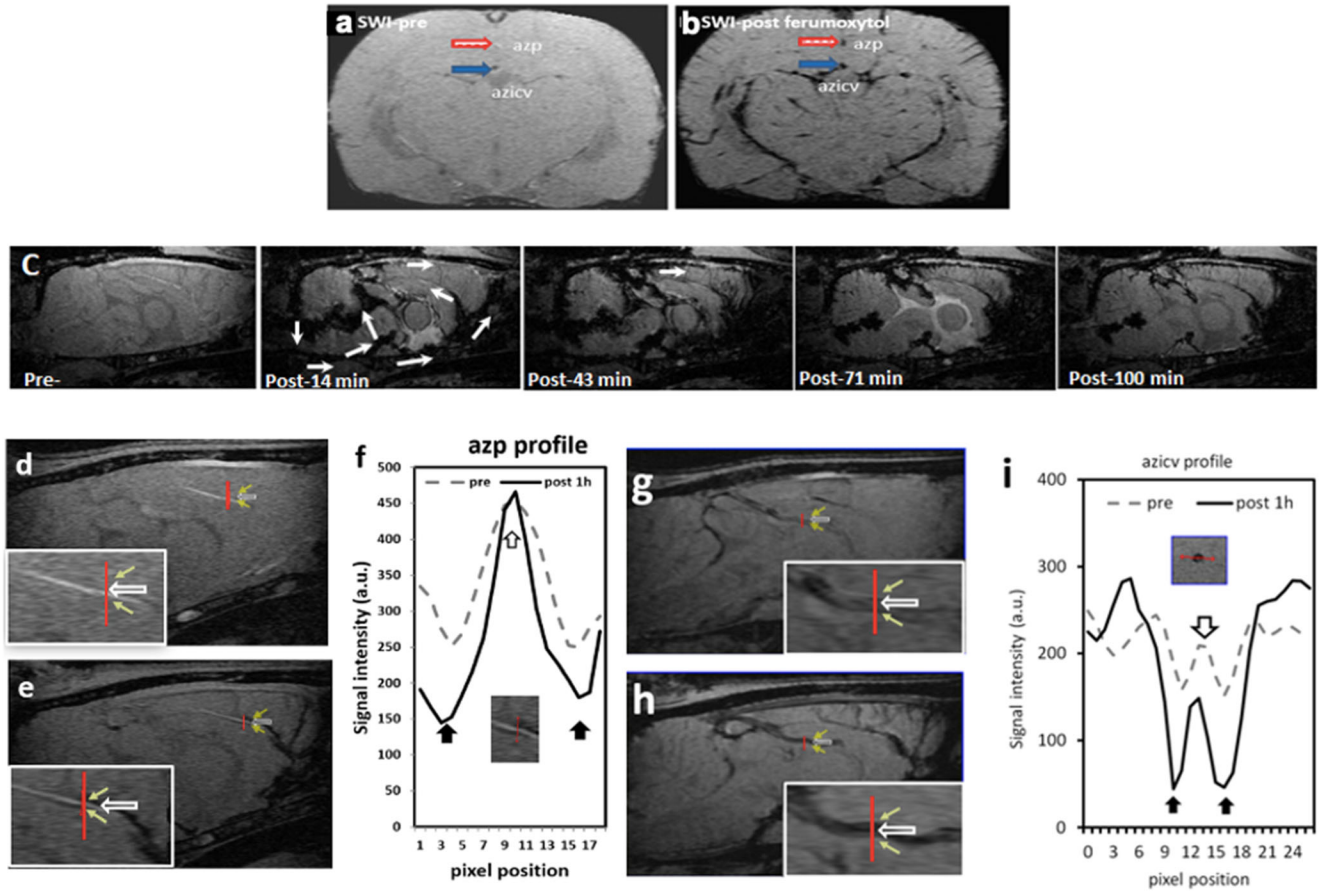

Fig. 2 MRI tracers injected into the CSF in rats are cleared into the parenchymal veins. **a**, **b** Distinguishing cerebral arteries and veins on SWI post-intravenous Ferumoxytol injection. **a** Baseline pre-injection: azygos pericallosal artery (azp, red arrows) shows slight hyperintense (bright) on SWI representing an inflow effect, but the azygos internal cerebral vein (azicv, blue arrows) shows hypointense (dark) due to the presence of deoxyhemoglobin. **b** 15 min post-injection: both artery and vein show hypointense on SWI due to the iron-based contrast agent. **c** Dynamic CSF tracer (240 μg (Fe) Ferumoxytol infusion via cisterna magna) changes over time demonstrating early tracer influx (0–43 min) followed by tracer clearance (43–100 min, white arrows indicate tracer flow). **d**–**i** Distinguishing para-vascular vs intra-vascular spaces post-Fe-Dextran CSF infusion for a representative rat. **d**, **e** Sagittal pre- and 1-h post-ICM SPIO-SWIs (1st echo) of the azygos pericallosal artery (azp, empty arrow) are bright (hyperintense) while para-arterial spaces (mustard arrows) are dark (hypointense). **f** azp cross-sectional signal intensity profiles pre- and post-SPIO at 1-h time points (profile locations indicated by red lines in **d** and **e**; black arrows: para-arterial space; empty arrow: azp). **g**, **h** Sagittal pre- and 1-h post-ICM SPIO-SWIs (2nd echo) of the azygos internal cerebral vein (azicv, empty arrows); mustard arrows: para-venous spaces. **i** azicv cross-sectional signal intensity profiles pre- and post-SPIO at 1-h time points show temporal changes in the MR signal intensities (profile locations indicated by red lines in **g** and **h**); empty arrow: azicv; black arrows: para-venous spaces. CSF tracer entered in the azicv but not azp via ICM infusion

original image resolution of 41.6 × 83.2 × 160 μm^3); one average; and an acquisition time of 30 min. The 30-min 3D SWI sequence was continuously acquired for 2 h, that is, one baseline scan followed by ICM infusion of the tracer and three post-contrast scans. After 2 h, the 3D scan was repeated 2 to 3 times at a longer interval of 45 min with two other inserted sequences (a coronal MR angiogram and a 3D T1-weighted imaging) unrelated to this study. The post-contrast time was determined from the beginning of the infusion to the middle of each scan.

MRI data analysis MRI data were processed using in-house software Signal Processing in NMR (SPIN) (http://www.mrc.wayne.edu/). The quantitative susceptibility mapping (QSM) was obtained similar to that presented in a previous publication [25]. The increase in the susceptibility is directly proportional to the amount of SPIO tracer present [28]. Arterial-related parameters were measured using the first echo images with better time-of-flight effects to highlight the arteries while the venous system was evaluated using the second echo images which provide better susceptibility effects and hence better visualization of the veins. 3D regions-of-interest (ROIs) were drawn manually on zoomed images (8 × in each direction in plane, zoom type: Fourier Windowed Sinc Interpolated) for the azygos pericallosal artery (azp), azygos internal cerebral vein (azicv), and corresponding para-

vascular space. The MRI signal intensity (SI) was measured as an average over all voxels in the 3D-ROIs (28 ± 7 slices for the azp covering from the genu to the splenium of the corpus callosum, 14 ± 3 slices for the azicv covering from the end of the dorsal septal vein to the great cerebral vein of Galen). The corresponding volume was measured from the product of the number of voxels and a single voxel volume. Since the number of slices was the same for pre- and post-images in a given 3D-ROI, the ratio of the cross-sectional areas equals the corresponding volume ratio. Vascular susceptibility values (in parts per billion, ppb) were measured from the 3D-ROIs using the above SI method from the QSM data. The venous pixels were carefully selected to avoid touching the edges of the neighboring very small para-venous spaces. Since the artery had low susceptibility, it was measured at longer echo times based on the 3D-ROIs obtained from the first echo magnitude images. In order to reduce the effect of potential variations in scale factor from scan to scan, the relative changes of the SI (in percent) were used as follows: $100 \times (SI(t)-SI(0))/SI(0)$, where SI(0) refers to the SI at the pre-contrast time point, and SI(t) to the post-contrast time points. The percentage changes in signal were averaged over four post-contrast time points (15, 45, 75, and 120 min) in the evaluation of the tracer clearance rate between the azicv and its peri-venous space.

Statistical analysis

Data are presented as mean (± SE), while SI or susceptibility or their relative changes in percent are plotted as bar and line graphs, as appropriate. Two-tailed, paired sample t-tests were used to compare baseline to post-tracer signal intensity measurements. Statistical significance was established at p values less than the critical alpha value of 0.05. All statistics were performed using Microsoft Excel.

Results

Visualization of arteries and veins using the SPIO-SWI method

The SPIO-SWI method was able to distinguish parenchymal arteries and veins in all 5 rats (Fig. 2a, b) under i.v. injection of Ferumoxytol at a dose of 5.6 mg/kg. Dynamic tracer changes using the SPIO-SWI method under ICM infusion of 240 μg Fe for all 5 rats (Fig. 2c) were consistent with published CSF pathways seen with other imaging methods [1, 5, 7, 9, 29]. The capability of simultaneously distinguishing the artery, vein, and their corresponding para-vascular space is illustrated in Fig. 2d–i under ICM infusion of Fe-Dextran at a quantity of 100 μg Fe.

CSF tracer entry into the parenchymal veins

Qualitative results We first qualitatively evaluated whether the amount of MRI tracers in the brain parenchymal veins was more than that in the brain parenchymal arteries (Fig. 2d–i). Figure 2f clearly demonstrates that the MRI tracers flowed along the para-arterial space but did not enter the arterial blood: the intensity of the peak signal from the azp remained virtually unchanged with time, while the intensities of the two valleys (corresponding to the azp para-arterial space) decreased. In contrast, Fig. 2i shows that the MRI tracers flowed along the para-venous space and entered the venous blood: the peak signal intensities from the venous blood of the azicv decreased with time, indicating that the tracer in fact entered the azicv, unlike the azp; similar to the para-arterial space in Fig. 2f, the two dips in signal intensity (corresponding to the azicv para-venous space) indicate that the tracers flowed along the para-venous space. The mean (± SE) of the azp diameter was 0.15 (± 0.02) mm and the corresponding para-vascular space was 0.06 (± 0.03) mm. The mean (± SE) of the azicv diameter was 0.24 (± 0.02) mm and that of the corresponding para-vascular space was less than 0.040 (± 0.003) mm.

Quantitative results using relative changes in MRI signal intensity We quantitatively measured CSF tracer in both the azicv and azp using the SPIO-SWI method with 75 μg (Fe) FeREX™ (100 nm) tracer, via ICM infusion. The relative signal intensity changes (mean (± SE)%) in the venous ROI (vROI) of the azicv decreased by 16.0 (± 4.1)% at 15 min post-tracer infusion compared to baseline (pre-tracer) ($p < 0.01$) ($n = 5$) (Fig. 3a). Similar findings were observed with 270 μg (Fe): in this case, the signal decreased by 10.8 (± 2.5)% in the azicv ($p = 0.02$) ($n = 5$) (Fig. 3b). In contrast, the relative changes (%) in signal intensity in the arterial region-of-interest (aROI) of the azp were not significantly different using the 75 μg (Fe) FeREX™ (100 nm) tracer, via ICM infusion ($p = 0.8$) ($n = 5$) (Fig. 3a). However, we did observe changes in the aROI when using the 270 μg (Fe) (Fig. 3b); the relative decrease in SI in the aROI was 9.1 (± 2.8)% ($p = 0.04$) ($n = 5$) (Fig. 3b). Similar results were obtained using a smaller MRI tracer, Ferumoxytol (17–31 nm) ($n = 5$) (Fig. 3c, d). The relative decrease in the SI for the aROI of the azoxytol via ICM infusion ($p = 0.051$) ($n = 5$) (Fig. 3c), which was larger than that of FeREX although both of them were not significantly different from zero.

Quantitative results using QSM data Susceptibility of the CSF tracer was measured in both the azicv and azp. Figure 4a shows that the CSF tracers entered the azicv with the 75 μg (Fe) FeREX™ (100 nm) tracer via ICM infusion; the relative

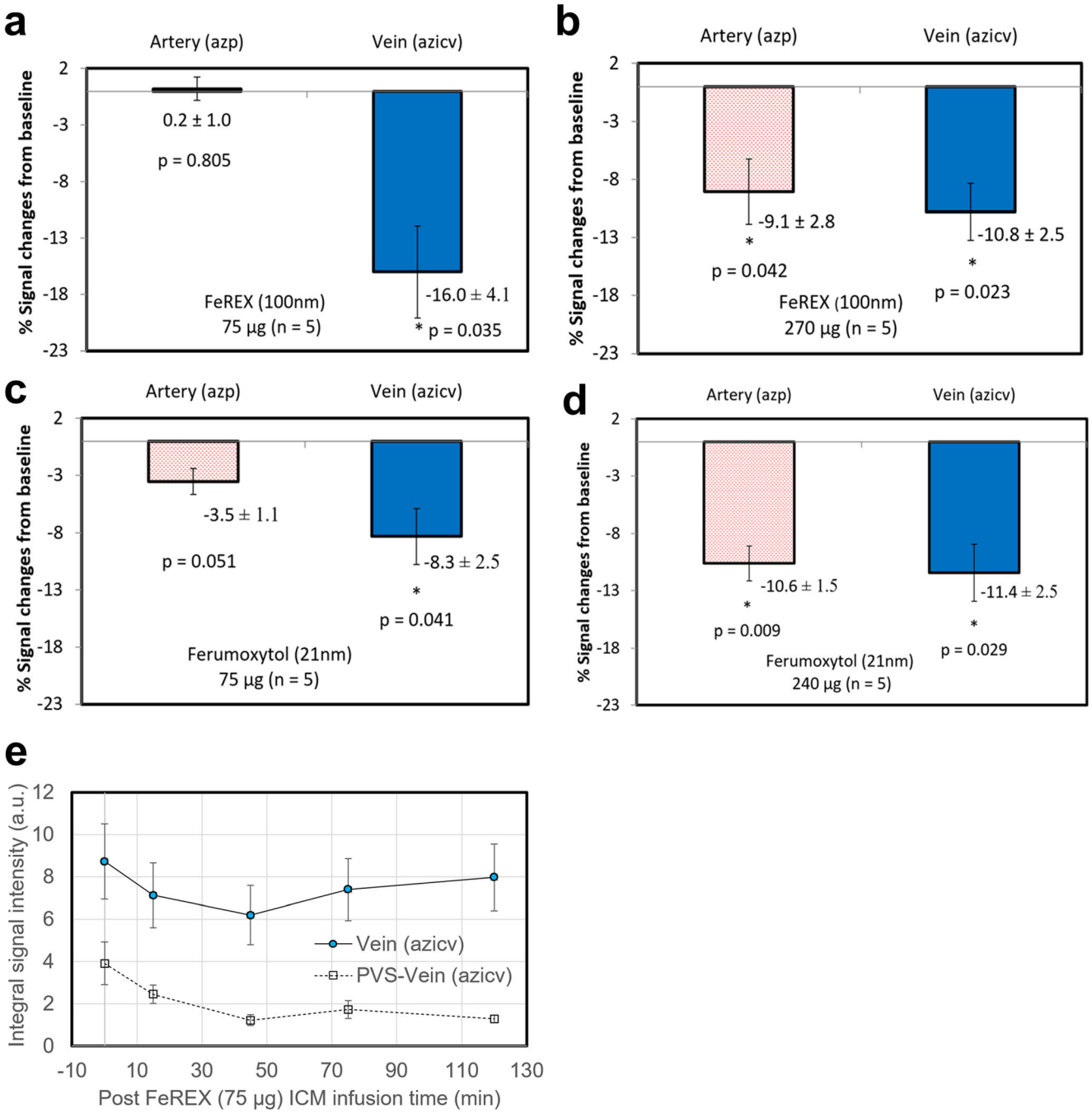

Fig. 3 Participation of the parenchymal venous pathway in CWC shown by SWI post-SPIO CSF tracer infusion in normal rats. **a**, **b** Relative changes (%) in MRI signal intensity pre/post 75 µg (Fe) (**a**) and 270 µg (Fe) (**b**) FeREX™ (100 nm) in azygos pericallosal artery (azp) and azygos internal cerebral vein (azicv), demonstrating CSF tracer presence in the azicv, but not the azp, with a low dose of iron. **c**, **d** Quantitative relative changes (%) in MRI signal intensity pre/post 75µg (**c**) and 240 µg (**d**) Ferumoxytol in azp and azicv, demonstrating CSF tracer presence in the azicv, but not in the azp, at a low dose of iron. **e** Temporal MRI integral signals (mean ± SE) in the azicv and its corresponding para-venous space (pvs) for the 75 µg (Fe) FeREX ($n = 5$). The estimated percent changes in the integral signal averaged over four time points (2 h) was −18 (± 7)% for the vein and −57 (± 13)% for its corresponding para-vascular space. This gave an estimate of a ratio of 32:100 for FeREX percentage drainage from the vein and its corresponding PVS without the consideration of the difference in their circulation speed

increase in susceptibility was 13.5 (± 1.0)% at 15 min post-tracer infusion ($p < 0.01$) and 33.6 (± 6.7)% at 45 min post-tracer infusion ($p = 0.01$), compared to baseline (pre-tracer) ($n = 5$). In contrast to the parenchymal veins, negligible amounts of CSF tracers entered the azp: 1.3 (± 2.6)% at 15 min post-tracer infusion ($p = 0.6$), and 12 (± 19)% at 45 min post-tracer infusion ($p = 0.5$), compared to baseline (pre-tracer) (Fig. 4b).

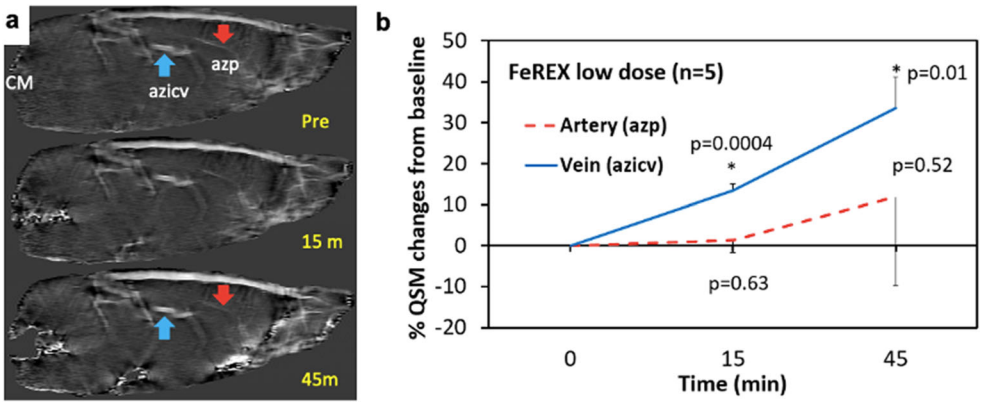

Fig. 4 Temporal relative changes in QSM with 75 μg (Fe) FeREX. QSM relative changes (%) pre-, post-15min, and post-45min 75 μg (Fe) FeREX™ (100 nm) CSF tracer in the azygos pericallosal artery (azp) and the azygos internal cerebral vein (azicv), demonstrating CSF tracer presence in the azicv, but not the azp at 75 μg (Fe). **a** An example rat mid-sagittal QSM image for pre-, post-15 min, and post-45 min CSF tracer showing a representative vein (azicv, arrows blue and upward) and artery (azp, arrows red and downward). **b** Plot of the percent QSM change from baseline over time for a select parenchymal artery (azp) and vein (azciv) (n = 5)

Substantial contribution of the parenchymal venous pathway to MRI tracer clearance

We then determined whether the parenchymal venous pathway plays a substantial role in CWC as compared to the perivenous CSF pathway. Figure 3e shows the temporal changes in the integral signal intensity of the azicv and its corresponding peri-venous space over a 2-h time period (n = 5, 18 slices per rat) at the 75 μg (Fe) FeREX. The ratio of the average percentage change in signal over four post-contrast time points for the azicv versus the para-venous space was 32:100, without the consideration of the differences in the rates of circulations of blood and CSF.

Discussion

Due, in part, to the lack of convincing evidence, most studies on CWC do not discuss the possibility of the brain parenchymal vascular contribution, even though it has been recognized that "if there is a transport mechanism for a substance at the BBB, then the BBB is more important than peri-vascular pathways for the elimination of that substance," because the circulation speed of the vascular system is more than one order faster than that of CSF [21]. The SPIO-SWI method makes it possible to simultaneously evaluate both influx and efflux pathways of the parenchymal vascular system as well as the CSF system with different sizes and concentrations of MRI tracers. In this work, we have demonstrated quantitatively that there is a net brain parenchyma-to-blood efflux of MRI tracers into the venous system following ICM infusion of a tracer.

Other papers have reported that a large portion of the tracer entering the blood stream from the CNS and only a relatively small fraction of CSF tracer drain via the lymphatic channels [9, 15–17]. The traditional explanation of the CSF tracer getting into the circulation blood pool is focused on the arachnoid villi [30–32]. However, this concept has been questioned based on light microscopic examinations [9, 15, 18]. Our results provide an alternative explanation of this unanswered question. Our study confirmed that the parenchymal venous pathway can contribute substantially to CWC. The ratio of the average percentage change in signals for the vein (azicv) versus the para-venous space was about 32:100. A value greater than zero indicates the participation of the vein system in CWC. This ratio would be further increased when considering the differences in flow rate between the blood (2 mL/min) and the CSF (3.7 μL/min) [33, 34]. That is, the brain parenchymal venous system plays a substantial role in the clearance of cerebral MRI tracers in addition to the CSF system (accounting for this flow ratio difference would change this ratio to more than 10).

The ICM MRI tracers in the CSF can drain into the systemic blood circulation. Only the residual re-circulating tracers remaining after the systemic removal by the liver, spleen, and other waste clearance organs will be pumped back into the blood and enter the arteries. At 240 or 270 μg (Fe) tracer, we observed the CSF FeREX™ tracer in both the parenchymal arteries and veins, most likely indicating residual systemic blood re-circulation of tracer, as opposed to direct entry into the parenchymal arteries. An average adult rat (~300 g) has a total blood volume about ~19 mL and a total CSF volume of about ~0.58 mL (cisterna magna ~0.19 mL) [35–37]. With a CSF tracer quantity of 75 μg eventually draining into the systemic blood circulation (assuming complete drainage and without removal from the system), the concentration of tracer in the blood would be about ~3.95 μg/mL (75 μg divided by 19 mL), about 3% of the initial CSF tracer concentration. Considering tracer removal from the systemic circulation by the reticuloendothelial system of the liver, spleen, and bone marrow, the residual systemic tracer

concentration would be less [38]. Therefore, the residual systemic re-circulation of the tracer can be ignored at 75 μg (Fe) tracer quantity. However, at 270 μg (Fe) tracer quantity, the residual tracer concentration in the blood is about 4-fold higher, equivalent to a dose of 0.9 mg/kg (270 μg divided by 300g); this corresponds to one-quarter of the typical IV dose (4 mg/kg) used for T2*-weighted MRI scans, resulting in significant signal intensity change within the parenchymal arteries [25].

One might debate that the observation of the tracer entering the parenchymal veins is due to the blooming effects (imaging artifact) in the corresponding para-venous spaces. However, this argument can be excluded by the observation that no tracer was detected in or around the arteries when 75 μg (Fe) tracer was used.

The finding that MRI tracers can enter the parenchymal venous system but not the parenchymal arterial system is logically consistent with the well-known differences in the anatomical structures and functions between the venous and arterial systems. The observation of the venous removal of the MRI tracers is consistent with the notion that tissue in the human body drains about 90% of the interstitial fluid through the venous system and the remaining 10% through the lymphatic system [39]. Considering the brain is the most bioactive, energy-consuming organ (20% nutrition for about 5% of body weight) in the body [40], it is illogical that the brain would rely on the slow CSF circulation for CWC while less bioactive tissues outside the brain require both the fast vascular and slow lymphatic systems to remove waste in a timely manner [19]. The size of the BBB is smaller than the USPIO used here. The transcytosis can transport large substrates across the BBB but the amount of USPIO detected in the blood pool seems large than that from transcytosis. The mechanism behind this observation is unknown and warrants further investigation.

The direct participation of the parenchymal venous system also questions our traditional understanding of the role of arachnoid granulations in CWC. CSF involved with CWC drains outside the brain parenchyma into the systemic blood circulation via two routes, either directly through dural venous sinuses via arachnoid granulations or indirectly through lymphatic pathways [41–43]. While there is a general consensus on the two routes, the magnitude of each route's involvement was brought into question by previous studies [9, 15–18]. Welch et al reported that 5 h after the injection of albumin dye into the CSF space of rabbits only 5% was seen draining into the cervical lymph nodes [17]. This finding led to the conclusion that only a small fraction of CSF drains via the lymphatic channels. However, in the same period of time only 14% of the injected dye was found in the blood, revealing that lymphatic channels contributed up to 26% of the tagged protein that had left the central nervous system and entered the blood stream [16]. The CSF tracer entering blood stream is most notable across the arachnoid villi/granulations [30–32]. However, their results were questioned since the dye was injected at a pressure of up to 60 mmHg. High pressure during the dye injection could cause rupture of the arachnoid villi/granulations and absorption into the sinuses [31]. These studies have cast doubt on this understanding, inviting scientists to rethink the exact role and magnitude of the arachnoid villi/granulation route. Previously published work indicates that the superior sagittal sinus was not a significant draining channel in normal and hydrocephalic rats, as evidenced by much lower signal intensity changes on MRI in the superior sagittal sinus versus the azygos internal cerebral vein, following lateral ventricle injection of tracer [9]. Logically, if waste in the brain parenchyma can directly enter the parenchymal venous system, and since blood circulation is much faster than the CSF circulation, we can reasonably surmise that the arachnoid granulations, which are located outside the brain parenchyma, are at most, if at all, only a secondary pathway for CWC.

Beside the signal loss associated with the iron-based contrast agents, for low concentrations, we have also observed positive signal enhancement in the vessels in the rat brain using the SWI sequence at short echo times as would be expected from the T1 enhancing nature of these agents. However, for higher concentrations this effect is overcome by the large T2* relaxivity of the agents. Also, we should note that the susceptibility results from QSM are independent of signal magnitude.

This study has several limitations. First, it does not investigate all influx arterial vessels and all efflux venous vessels. Second, it does not investigate the underlying mechanism for how the MRI tracers enter the vascular system. Third, rats may have different physiological waste clearance than humans. The CWC in humans is much slower than that in rats and after injection reaches a peak at ~10 h compared with ~ 2 h in rats [5, 44]. Therefore, the whole CWC in humans needs to be monitored over 1–2 days [45, 46]. We also do not consider the waste clearance pathway or how waste drains or moves in and out the brain to avoid possible confusion. We are designing experiments to address these issues in the future. Fourth, we cannot exclude the possibility that prolonged anesthesia could impact the physiological status of the animal and affect the results. However, these effects on BBB permeability, if any, are likely small and to-date there are no reports demonstrating significant changes of BBB permeability due to extended anesthesia. Fifth, a constant quantity of contrast agent was used in the rats (body weights ranging from 350 to 450 g). It would be better to use a constant dose in the future. Finally, we used anisotropic spatial resolution in QSM due to imaging time and signal-to-noise considerations. This should not affect our results significantly since we use relative changes in susceptibility rather than absolute values.

In summary, using a state-of-art MR imaging technique with iron-based contrast agents, we observed that not only

MRI CSF tracers entered the parenchymal veins, but also the parenchymal venous system contributed substantially to the cerebral clearance of these tracers. These results challenge the traditional understanding of the role of arachnoid granulations in CWC. In conclusion, the parenchymal venous system appears to participate directly in CWC and complements the established CSF pathways.

Funding This work was supported in part by the National Institutes of Health (NIH) Grant, RF1-AG057494, R01-NS108463 and R01-NS108491.

Declarations

Guarantor The scientific guarantor of this publication is Quan Jiang.

Conflict of interest The authors of this manuscript declare no relationships with any companies whose products or services may be related to the subject matter of the article.

Statistics and biometry No complex statistical methods were necessary for this paper.

Informed consent All experimental animal procedures were conducted in accordance with the National Institutes of Health (NIH) Guide for the Care and Use of Laboratory Animals and approved by our Institutional Animal Care and Use Committee (IACUC) of Wayne State University.

Ethical approval Institutional Review Board approval was not required because this study was conducted on animals.

Methodology
- Prospective
- Experimental
- Performed at one institution

References

1. Iliff JJ, Wang M, Liao Y et al (2012) A paravascular pathway facilitates CSF flow through the brain parenchyma and the clearance of interstitial solutes, including amyloid beta. Sci Transl Med 4:147ra111
2. Rangroo Thrane V, Thrane AS, Plog BA et al (2013) Paravascular microcirculation facilitates rapid lipid transport and astrocyte signaling in the brain. Sci Rep 3:2582
3. Plog BA, Dashnaw ML, Hitomi E et al (2015) Biomarkers of traumatic injury are transported from brain to blood via the glymphatic system. J Neurosci 35:518–526
4. Mestre H, Tithof J, Du T et al (2018) Flow of cerebrospinal fluid is driven by arterial pulsations and is reduced in hypertension. Nat Commun 9:4878
5. Jiang Q, Zhang L, Ding G et al (2017) Impairment of the glymphatic system after diabetes. J Cereb Blood Flow Metab 37:1326–1337
6. Louveau A, Da Mesquita S, Kipnis J (2016) Lymphatics in neurological disorders: a neuro-lympho-vascular component of multiple sclerosis and Alzheimer's disease? Neuron 91:957–973
7. Jessen NA, Munk AS, Lundgaard I, Nedergaard M (2015) The glymphatic system: a beginner's guide. Neurochem Res 40:2583–2599
8. Arbel-Ornath M, Hudry E, Eikermann-Haerter K et al (2013) Interstitial fluid drainage is impaired in ischemic stroke and Alzheimer's disease mouse models. Acta Neuropathol 126:353–364
9. Krishnamurthy S, Li J, Shen Y, Duncan TM, Jenrow KA, Haacke EM (2018) Normal macromolecular clearance out of the ventricles is delayed in hydrocephalus. Brain Res 1678:337–355
10. Xie L, Kang H, Xu Q et al (2013) Sleep drives metabolite clearance from the adult brain. Science 342:373–377
11. Iliff JJ, Wang M, Zeppenfeld DM et al (2013) Cerebral arterial pulsation drives paravascular CSF-interstitial fluid exchange in the murine brain. J Neurosci 33:18190–18199
12. Louveau A, Smirnov I, Keyes TJ et al (2015) Structural and functional features of central nervous system lymphatic vessels. Nature 523:337–341
13. Albargothy NJ, Johnston DA, MacGregor-Sharp M et al (2018) Convective influx/glymphatic system: tracers injected into the CSF enter and leave the brain along separate periarterial basement membrane pathways. Acta Neuropathol 136:139–152
14. Carare RO, Bernardes-Silva M, Newman TA et al (2008) Solutes, but not cells, drain from the brain parenchyma along basement membranes of capillaries and arteries: significance for cerebral amyloid angiopathy and neuroimmunology. Neuropathol Appl Neurobiol 34:131–144
15. Brinker T, Stopa E, Morrison J, Klinge P (2014) A new look at cerebrospinal fluid circulation. Fluids Barriers CNS 11:10
16. McComb JG (1983) Recent research into the nature of cerebrospinal fluid formation and absorption. J Neurosurg 59:369–383
17. Courtice FC, Simmonds WJ (1951) The removal of protein from the subarachnoid space. Aust J Exp Biol Med Sci 29:255–263
18. Eide PK, Mariussen E, Uggerud H et al (2021) Clinical application of intrathecal gadobutrol for assessment of cerebrospinal fluid tracer clearance to blood. JCI Insight 6
19. Sherwood L (2010) Human physiology: from cells to systems, 7th edn.
20. Haughton VM, Korosec FR, Medow JE, Dolar MT, Iskandar BJ (2003) Peak systolic and diastolic CSF velocity in the foramen magnum in adult patients with Chiari I malformations and in normal control participants. AJNR Am J Neuroradiol 24:169–176
21. Hladky SB, Barrand MA (2018) Elimination of substances from the brain parenchyma: efflux via perivascular pathways and via the blood-brain barrier. Fluids Barriers CNS 15:30
22. Wang H, Jiang Q, Shen Y et al (2020) The capability of detecting small vessels beyond the conventional MRI sensitivity using iron-based contrast agent enhanced susceptibility weighted imaging. NMR Biomed. https://doi.org/10.1002/nbm.4256:e4256
23. Liu S, Brisset JC, Hu J, Haacke EM, Ge Y (2018) Susceptibility weighted imaging and quantitative susceptibility mapping of the cerebral vasculature using ferumoxytol. J Magn Reson Imaging 47:621–633
24. Haacke EM, Xu Y, Cheng YC, Reichenbach JR (2004) Susceptibility weighted imaging (SWI). Magn Reson Med 52:612–618
25. Shen Y, Hu J, Eteer K et al (2020) Detecting sub-voxel microvasculature with USPIO-enhanced susceptibility-weighted MRI at 7 T. Magn Reson Imaging 67:90–100
26. Ding G, Chopp M, Li L et al (2018) MRI investigation of glymphatic responses to Gd-DTPA infusion rates. J Neurosci Res 96:1876–1886
27. Iliff JJ, Lee H, Yu M et al (2013) Brain-wide pathway for waste clearance captured by contrast-enhanced MRI. J Clin Invest 123:1299–1309

28. Haacke EM, Liu S, Buch S, Zheng W, Wu D, Ye Y (2015) Quantitative susceptibility mapping: current status and future directions. Magn Reson Imaging 33:1–25
29. Johnston M, Zakharov A, Papaiconomou C, Salmasi G, Armstrong D (2004) Evidence of connections between cerebrospinal fluid and nasal lymphatic vessels in humans, non-human primates and other mammalian species. Cerebrospinal Fluid Res 1:2
30. Davson H, Domer FR, Hollingsworth JR (1973) The mechanism of drainage of the cerebrospinal fluid. Brain 96:329–336
31. Johanson CE, Duncan JA 3rd, Klinge PM, Brinker T, Stopa EG, Silverberg GD (2008) Multiplicity of cerebrospinal fluid functions: new challenges in health and disease. Cerebrospinal Fluid Res 5:10
32. Davson H (1966) Formation and drainage of the cerebrospinal fluid. Sci Basis Med Annu Rev:238–259
33. Larkin JR, Simard MA, Khrapitchev AA et al (2019) Quantitative blood flow measurement in rat brain with multiphase arterial spin labelling magnetic resonance imaging. J Cereb Blood Flow Metab 39:1557–1569
34. Yaksh TL (1999) Spinal systems and pain processing: development of novel analgesic drugs with mechanistically defined models. Trends Pharmacol Sci 20:329–337
35. Lee HB, Blaufox MD (1985) Blood volume in the rat. J Nucl Med 26:72–76
36. Lai YL, Smith PM, Lamm WJ, Hildebrandt J (1983) Sampling and analysis of cerebrospinal fluid for chronic studies in awake rats. J Appl Physiol Respir Environ Exerc Physiol 54:1754–1757
37. Nirogi R, Kandikere V, Mudigonda K et al (2009) A simple and rapid method to collect the cerebrospinal fluid of rats and its application for the assessment of drug penetration into the central nervous system. J Neurosci Methods 178:116–119
38. Mukundan S, Steigner ML, Hsiao LL et al (2016) Ferumoxytol-enhanced magnetic resonance imaging in late-stage CKD. Am J Kidney Dis 67:984–988
39. Schwartz N, Chalasani MLS, Li TM, Feng Z, Shipman WD, Lu TT (2019) Lymphatic function in autoimmune diseases. Front Immunol 10:519
40. Camandola S, Mattson MP (2017) Brain metabolism in health, aging, and neurodegeneration. EMBO J 36:1474–1492
41. Weed LH (1914) Studies on cerebro-spinal fluid. No III : the pathways of escape from the subarachnoid spaces with particular reference to the Arachnoid Villi. J Med Res 31:51–91
42. Ma Q, Ineichen BV, Detmar M, Proulx ST (2017) Outflow of cerebrospinal fluid is predominantly through lymphatic vessels and is reduced in aged mice. Nat Commun 8:1434
43. Pollay M (2010) The function and structure of the cerebrospinal fluid outflow system. Cerebrospinal Fluid Res 7:9
44. Watts R, Steinklein JM, Waldman L, Zhou X, Filippi CG (2019) Measuring glymphatic flow in man using quantitative contrast-enhanced MRI. AJNR Am J Neuroradiol 40:648–651
45. Eide PK, Ringstad G (2018) Delayed clearance of cerebrospinal fluid tracer from entorhinal cortex in idiopathic normal pressure hydrocephalus: a glymphatic magnetic resonance imaging study. J Cereb Blood Flow Metab. https://doi.org/10.1177/0271678X18760974:271678X18760974
46. Ringstad G, Vatnehol SAS, Eide PK (2017) Glymphatic MRI in idiopathic normal pressure hydrocephalus. Brain 140:2691–2705